DEBRIS CLOUD ANALYTICAL PROPAGATION FOR A SPACE ENVIRONMENTAL INDEX

Francesca Letizia[*], *Camilla Colombo*, *Hugh G. Lewis*

University of Southampton
Astronautics Research Group
Southampton, SO17 1BJ
United Kingdom

Holger Krag

ESA Space Debris Office
ESOC
Darmstadt, 64293, Germany

ABSTRACT

An environmental index for spacecraft and rocket bodies is proposed. It considers how the fragment cloud generated by the breakup of a space object would affect the collision probability for operational satellites. The proposed index is computed by defining a grid in semi-major axis, inclination, and mass of synthetic fragmenting objects. An analytical method is used to propagate the resulting debris cloud and to compute the collision probability for a set of target spacecraft. Finally, the index for a generic space object is derived by interpolation of the values obtained on the grid. The results obtained applying the index definition to the objects in the DISCOS database are shown, together with a comparison to other formulations available in literature and a discussion on possible application of the index.

Index Terms— space debris, environmental index, debris cloud

1. INTRODUCTION

The long term evolution of the space debris environment is highly affected by fragmentations of massive objects, such as intact large spacecraft and rocket bodies [1]. Different metrics have been proposed to rank spacecraft depending on the consequences of their fragmentation on the space environment. The purpose of these analyses is to obtain a deeper insight on the critical parameters that have the largest influence on the space debris evolution. In addition, the output of these rankings could lead to the identification of potential candidates for active debris removal missions where it would be important to decide which spacecraft should be removed first to have the largest global beneficial effect.

Several authors have proposed different approaches to the problem and highlighted the relevance of having a quantitative measure of the environmental effect of an object in orbit, depending on its orbital parameters and physical characteristics [2, 3, 4, 1]. Rossi et al. [5], for example, simulated different fragmentations, considering locations and targets representative of the distribution of intact objects in orbit. For each scenario, the number of objects present in orbit in the 200 years following the fragmentation was studied and used to measure the effect of the fragmentation. Alternatively, Rossi et al. [1] introduced a *criticality* index, which depends on the background debris density, the object residual lifetime, the mass, and its orbital inclination. Similar parameters were identified also by Utzmann et al. [2]. In these case, no simulation is performed, and the indices collect what are identified as the most relevant factors to provide an immediate measure of the criticality of the studied space object. A different approach was presented by Lewis [6], where the proposed environmental index is computed considering the spacecraft orbital region, the implementation of mitigation measures for the spacecraft and their long term effect.

These examples show how the proposed environmental indices focus on different aspects of the space debris environment, ranging from the likelihood of the breakup to happen to the evaluation of the long-term changes in the whole debris population. In the ECOB index (Environmental Consequences of Orbital Breakups) proposed in this work, only the effects of potential breakups, of spacecraft and rocket bodies, are studied. Their effect is measured by the resulting collision probability for a set of target spacecraft. A grid in semi-major axis, inclination, and mass is used to define possible initial conditions of the breakup. For each case, the evolution of the produced debris cloud is modelled applying an analytical method, which describes how the cloud density changes under the effect of atmospheric drag. Given the evolution in time of the fragment density, the collision probability of the targets with the cloud is obtained applying the analogy with

[*]Francesca Letizia would like to acknowledge the support of the Institution of Engineering and Technology to organise a visiting period at ESA Space Debris Office. The authors thank Jan Siminski and Stijn Lemmes, from the ESA Space Debris Office, for their support, and Dr. Sergio Ventura, from ESA Independent Safety Office, for his precious feedback on the index formulation. The authors acknowledge the use of the IRIDIS High Performance Computing Facility, and associated support services at the University of Southampton, in the completion of this work. Part of this work was funded by EPSRC DTP/CDT through the grant EP/K503150/1.

the kinetic theory of gases. Once the value of the index is know for any grid point, a simple interpolation can be used to compute the value of the index for any object.

2. DEBRIS CLOUD PROPAGATION METHOD

According to the NASA breakup model [7], for each trackable object produced by a fragmentation there are millions of objects in the size range between $1\,\mathrm{mm}$ and $5\,\mathrm{cm}$. Considering these numbers, even low intensity fragmentations can easily produce thousands of objects, whose individual propagation would make simulations prohibitive in terms of computational resources. Evolutionary studies on the debris population usually deal with this issue by setting a cut-off fragment size at $10\,\mathrm{cm}$, so that only objects larger than this threshold are included in the simulations. However, when the impact of a single breakup is analysed, it could be relevant to include all objects that have the potential to interfere with other spacecraft, decreasing the threshold down to $1\,\mathrm{mm}$ or $1\,\mathrm{cm}$. This change in the scope of the analysis can be achieved by abandoning the evaluation of the single fragments' trajectories and studying the fragmentation cloud globally.

The propagation method CiELO (debris Cloud Evolution in Low Orbits) was developed with this aim: within this approach, the fragmentation cloud is described in terms of its spatial density, whose evolution in time under the effect of drag is obtained by applying the continuity equation. A detailed description of the method can be found in Letizia et al. [8], whereas only a brief overview of the approach is provided here.

The simulation of a fragmentation event starts with the modelling of the breakup, using the NASA breakup model [9, 7]. The evolution of the fragment cloud from this time instant is affected both by the dispersion of the energy among the fragments and the effect of orbit perturbations. Considering only the case of fragmentations in LEO, the Earth's oblateness spreads the fragments to form a band around the Earth. Once the band is formed, the atmospheric drag can be considered as the main perturbation and the continuity equation can be applied to obtain the cloud density evolution, following the approach firstly proposed by McInnes [10].

Compared to the formulation by McInnes [10], where the debris density is function of the radial distance from the Earth (r) only, the method was extended to express the cloud density as function of semi-major axis (a) and eccentricity (e) [11]. This extension results into an increase in the method applicability, so that the method is applicable to study fragmentations occurring between 700 and $800\,\mathrm{km}$. This means that the analytical method can be employed for the whole region where the majority of fragmentations occurred [12] and where the debris density is maximum.

By applying the continuity equation the distribution of fragments with semi-major axis and eccentricity is known at any time and it can be used to compute the collision probability for a spacecraft crossing the fragment cloud. This is done by applying the analogy with the kinetic theory of gases, so that the cumulative collision probability

$$p_c = 1 - \exp\left(-s\Delta v \sigma \Delta t\right)$$

depends on the fragments' spatial density s, the average relative velocity Δv between the spacecraft and the objects in the cloud, the collisional cross-section area σ and the time t. The fragments' spatial density s is obtained from the distribution of the fragments in semi-major axis and eccentricity, considering which is the probability of finding an object at a certain altitude given its orbital parameters [13]. In addition, a *scaling factor* is applied to take into consideration the distribution of the fragments with latitude. This aspect is important to identify configurations where the target spacecraft and the fragment cloud have similar maximum latitude; in these cases, the spacecraft crosses the cloud where the fragment density is maximum [14]. Similarly, an analytical expression can be derived also for the relative velocity Δv, taking into consideration the orbital configuration of the cloud and the crossing spacecraft [14]. In this way, a density-based approach is available to assess the consequences of a breakup, including the contribution of small debris fragments.

3. ENVIRONMENTAL INDEX

The ability of the analytical formulation to model large debris clouds with limited computational effort (both in terms of simulation time and RAM) makes it suitable to simulate a large number of breakup scenarios and build an environmental index based on the assessment of their consequences. In this work, the breakups of specific space objects are evaluated in terms of the effect on a set of *target* objects, which represent the active satellites in LEO. The analytical propagation method CiELO allows the space of the most relevant object parameters (i.e. altitude, orbital inclination, and mass) to be *mapped* onto a value of environmental index, so that the most critical breakup conditions, in terms of the effect on operational spacecraft, can be identified. This approach requires two steps. First, the potential sources of fragmentations and which kind of fragmentations to simulate should be defined. Second, the target set should be represented in such a way that the propagation of all the active satellites' trajectories is not required. The next Sections will explain how these tasks are performed. Observe that the structure of the index can be applied also with different cloud propagation methods, given that they can provide the cloud spatial density with time. As an example, the same index structure could be applied in GEO (Geosynchronous Earth Orbit), where different analytical propagation methods are available [15], to study fragmentations within the GEO protected region and in the GEO graveyard orbit.

3.1. Sources of fragmentation

To keep the severity index as general as possible, a large set of virtual fragmentations is created. In particular, a grid in semi-major axis, inclination, and spacecraft mass was used. The extremes of the grid in semi-major axis are limited by the applicability of the method: the highest limit is set equal to $1000\,\mathrm{km}$ as for higher altitudes it will not be justifiable to model the atmospheric drag and not the solar radiation pressure. The lowest limit depends on the analytical formulation used for the propagation, which is applicable to fragmentation above $700\,\mathrm{km}$ for a propagation period around 25 years [11]. For the mass of the fragmentation source, a grid between $100\,\mathrm{kg}$ and $10\,000\,\mathrm{kg}$ was defined. Observe that the only way to consider the effect of the fragmenting mass within the NASA breakup model requires simulating catastrophic collisions and not explosions or non-catastrophic collisions. For all the simulated collisions the breakup of a spacecraft (rather than a rocket body) is assumed, even if in the size range of interest the impact of this hypothesis is minimal[1]. The collision velocity is set equal to $10\,\mathrm{km\,s^{-1}}$, which is an average value for LEO and which was used also by Rossi et al. [5]. The mass of the colliding projectile is neglected. Using the NASA breakup model, the simulation of a catastrophic collision involving a mass equal to $1000\,\mathrm{kg}$ results in the generation of almost seven million fragments larger than $1\,\mathrm{mm}$. Even if the analytical formulation is only weakly dependent on the number of fragments, this large value results in a long computational time only for the initialisation of the cloud. For this reason, the lowest cut-off size of the fragments was set equal to $1\,\mathrm{cm}$ for the results discussed in this work.

3.2. Target set

The effect of the virtual fragmentations is assessed on a set of spacecraft targets. The selection of the possible targets follows an approach similar to the one proposed by Rossi et al. [5] to define representative fragmentations. The cross-sectional area A_c was identified as the most relevant parameter for a target. The distribution of cross-sectional area across the LEO region was studied; also in this case, the semi major axis was limited to $700\,\mathrm{km} \leq a \leq 1000\,\mathrm{km}$ as in the definition of the potential fragmentation sources, even if targets at lower altitudes may also be considered. DISCOS database is used to extract the data of satellites orbiting in this region. Only satellites launched in the last ten years are included in the list, assuming that this criterion filters out inactive spacecraft. The studied LEO region is divided into cells in semi-major axis and inclination, applying the same grid used for the discretisation of possible fragmentation sources. For each cell, the cumulative cross-sectional area $\sum A_c$ is computed. An example of this analysis is shown in Figure 1, where the cells with the highest $\sum A_c$ are the most *vulnerable* in case of fragmentations.

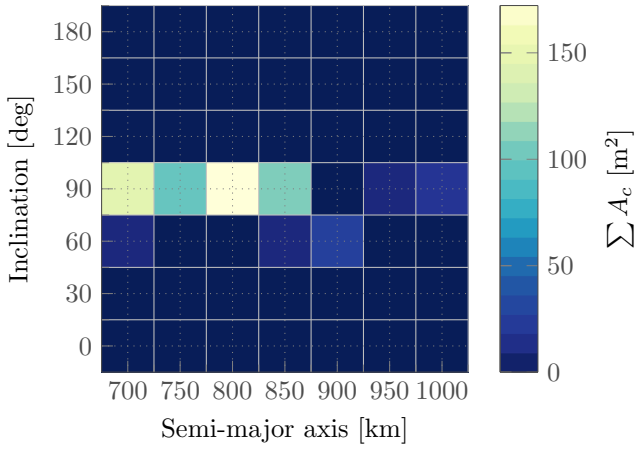

Fig. 1: Distribution of cross-sectional area in the cells in semi-major axis and inclination. Data from DISCOS.

Once the distribution of A_c is known, the target set can be defined by selecting for each cell in Figure 1 a *representative* spacecraft for which the collision probability is computed. As it will be shown later, the environmental index is obtained by combining the collision probability for each target, weighting their contribution depending on the share of A_c of the cell they represent. A fixed number of targets can be used or the code can select the appropriate number of targets to represent a given percentage of the total A_c. In the results shown in Section 5 the second approach is used, setting the percentage equal to 90% of the total A_c. The selection of targets is performed by defining a *synthetic* object with A_c and mass equal to the average values in the cell, semi-major axis and inclination equal to the centre of the cell.

3.3. Index definition

The purpose of the current analysis is to rank the *sources* of fragmentations evaluating their impact on a set of *targets* (i.e. the representative objects). As only the consequences of a breakup are evaluated, the proposed environmental index ECOB is defined as a simple sum of the collision probability on each target multiplied by the weighting factor, if used:

$$\mathrm{ECOB} = \sum_{j=1}^{N_{\mathrm{tar}}} w_j p_{c,j} \tag{1}$$

where

$$w_j = \frac{(A_c)_{\mathrm{cell},j}}{(A_c)_{\mathrm{tot}}} \tag{2}$$

is the ratio between the sum of A_c in the $j-$th cell and the total A_c on the whole target list; $p_{c,j}$ is the cumulative collision probability of the representative object of the $j-$th cell over the considered simulated time; N_{tar} is the total number

[1] The kind of object involved in the fragmentation affects the definition of the parameters of fragments larger than $8\,\mathrm{cm}$ only.

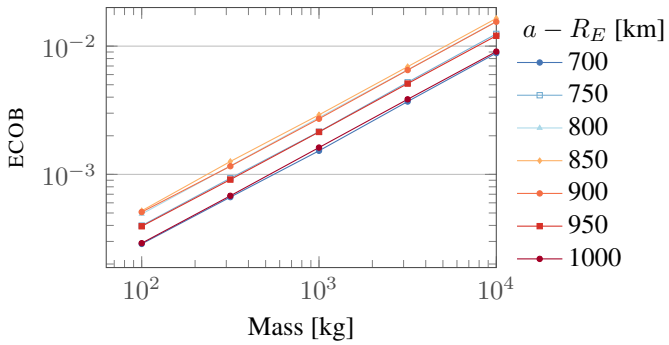

Fig. 2: Index dependence on the mass for different altitudes.

of representative objects. Observe that the w_j are constant for the whole simulation, meaning that it is assumed that for the whole simulated time span the distribution of cross-sectional area will be constant. This is equivalent to assume that, for the studied period, the space activities in the LEO region will be similar to the current ones.

3.4. Effect of the mass

As explained in Section 3, ECOB depends on the mass of the fragmentation that determines the number of fragments in the debris cloud and its spatial density. One simulation, with propagation time equal to 25 years, was run to evaluate the variation of the index with semi-major axis and breakup mass of the fragmenting object. Figure 2 shows the dependence of the index on the mass of the fragmenting space object for different altitudes and one can observe how the curve is a straight line in the log-log representation. In particular, it can be found that

$$\text{ECOB}(M) = \left(\frac{M}{M_{\text{ref}}}\right)^{0.75} \cdot \text{ECOB}(M_{\text{ref}}), \qquad (3)$$

where the exponent 0.75 is a direct results of the NASA breakup model. In fact, according to the model [9], the number of produced fragments larger than a given characteristic length is equal to

$$N_f(L_c) = 0.1(M)^{0.75} L_c^{-1.71}$$

with M equal to the sum of the target mass and the projectile mass in the case of catastrophic collisions.

4. INDEX COMPUTATION

The observation in Equation 3 is important because it allows the required number of simulations to be reduced, simplifying the computation of the index for a generic object. In fact, the index can be computed through simulations using a single reference value for the fragmentation mass (i.e. 10 000 kg) and a grid in semi-major axis and inclination.

4.1. Post-processing

The value of the index on the plane of semi-major axis and inclination, with a fixed value of mass, can be stored and scaled to the value of the mass of the analysed fragmenting object. Then, finding the value of the index at the semi-major axis and inclination of the analysed object becomes a problem of fitting the surface defined by the value of ECOB in the grid of semi-major axis and inclination. The advantage of this approach is that the computational effort is required only to generate the surface (which, as described in Section 3, is assumed to be *slowly*-changing if the development of space activities does not change abruptly). In this way, the reference surface is computed and stored, and severity index for all the objects in a database, such as DISCOS, can be quickly computed in post-processing, with a fitting procedure. Given the pairs $\{(\mathbf{x}_i^*, z_i^*)\}_i$, where $\mathbf{x}_i^*$ is a point of the grid in semi-major axis and inclination and z_i^* is the corresponding value of ECOB, the goal is to use these values to define a surface $Z = \{(\mathbf{x}_i, z_i)\}_i$ defined on the whole domain of semi-major axis and inclination. Three options for the fitting were identified and tested with MATLAB:

- interpolation, which finds the value z_i at each point $\mathbf{x}_i$ of the domain using the values z_i^* at the nearest grid points; the number of the considered near grid points depends on the interpolation scheme (e.g. bilinear, bicubic, biharmonic);
- local regression smoothing methods, which uses least squares regression techniques in combination with a weighting function that gives larger importance to closer data points when computing the value z_i of a generic point $\mathbf{x}_i$ in the domain[2];
- polynomial curve, which fits the data with a polynomial function in two dimensions.

In the case of interpolation, MATLAB offers different options for the curve to use (e.g. linear, cubic, or bi-harmonic spline). The interpolation does not give a strictly parametric expression of the surface Z, but a good representation of the surface. When regression methods are applied, the whole shape of the surface is described. In this case MATLAB offers two options for the regression model: a linear or a quadratic one. The description of the shape is good, but this method is not parametric, has a more complex formulation and does not seem to offer any additional advantage compared to the interpolation. For this reason, the regression methods were discarded. The third method, the polynomial curve, combines the positive features of the two previous approaches. Firstly, it describes the whole curve, so the coefficients needs to be computed only once and then the equation can be applied for

[2]A description of the method can be found at `http://uk.mathworks.com/help/curvefit/smoothing-data.html`, last access 5 January 2016.

the computation of the index for any object. Secondly, once the equation is obtained, it is completely independent from any programming language. However, the method tends to to *smooth* the curve, especially at the peak. For these reasons, the local interpolation was preferred.

4.2. Tool structure

The observations in the previous sections help defining the structure of the tool to compute the environmental index. This can be divided into two parts: first, the computation of index using a set of targets and a reference mass for the fragmentation on a predefined grid in semi-major axis and inclination; second, the computation of the index for different objects.

The first part of the tool uses the method based on the continuity equation and it is highly computationally expensive, so that the super-computer facilities of the University of Southampton, IRIDIS, were used. Once this phase is concluded, the output consists in a matrix of the index ECOB, computed on the defined grid, which can be easily saved and exported in different formats (e.g. `ASCII` file), depending on the user platform. The matrix represents the input of the code that actually computes the environmental index for the objects of interest. The code performs the fitting of the surface using a local interpolation method and rescaling the index depending on the mass of the studied objects. The code can receive as an input a file containing the list of the objects to analyse. For example, the results in Section 5 are obtained using as a database the data extracted from DISCOS [16] considering objects in orbits between 700 and 1000 km. For each object, its kind (i.e. rocket body, spacecraft, other) and its year of launch are specified, so that the user can choose to study only a subset of the list. A maximum number of the objects to study can also be specified.

4.3. Computational time

Some tests with a coarse grid were used to assess the computational time required by the simulations and identify the most effective parallelisation strategy to run cases with fine grids. Figure 3 shows the computational time for a case with $\Delta a = 50\,\mathrm{km}$, $\Delta i = 30\,\mathrm{deg}$. The computational time refers to a machine with 4 CPU; the whole code is written in MATLAB and exploits its built-in parallel statements (e.g. `parfor`). The histogram in Figure 3 shows the computational time for the three main functions in the code

- `propTarget` propagates the target trajectories considering atmospheric drag and J_2;
- `buildLayer` simulates a catastrophic collision for a given breakup mass in each cell and compute the cloud spatial density, including fragments down to 1 cm, for the whole desired time window
- `addCollProb` computes the collision probability for each target and the value of the index on the studied grid applying a weighting factor, if specified.

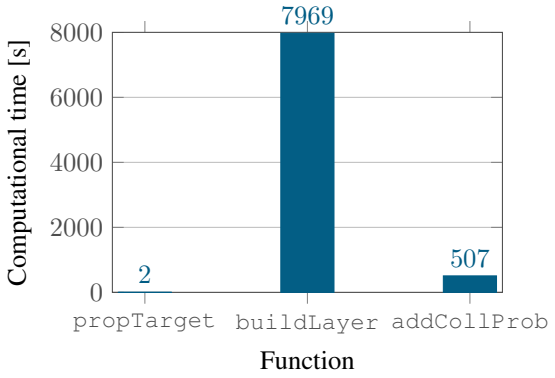

Fig. 3: Computational time on a PC with 4 CPU for a *layer* with coarse grid.

Applying the same settings to compute a case with a fine grid with $\Delta a = 10\,\mathrm{km}$, $\Delta i = 10\,\mathrm{deg}$ would require more than 22 hours of computation with 4 CPU (that is 3.6 days in CPU time) assuming that the simulation is still manageable in terms of RAM.

For this reason, it was decided to use IRIDIS, the super-computer facilities at the University of Southampton, to run the simulations with fine grids. The computation of one *layer* was divided into columns (simulations with the same semi-major axis), which are launched as separate jobs, each one with 12 processors allocated (the maximum). In this way one exploits not only the parallel features in MATLAB, but also the possibility of running multiple jobs at the same time. The submission of the jobs is fully automatised with a simple bash script. The whole setting allows a full layer to be obtained in a period of time between one and three hours (depending on the availability of processors on the server). The *real* computational time (summing the running time of each job) would be around 19 hours (equal to almost six days of CPU time).

5. RESULTS

Once the structure of the index was set, some simulations with a fine grid in semi-major axis ($\Delta a = 10\,\mathrm{km}$) and inclination ($\Delta i = 10\,\mathrm{deg}$) were run. Using a threshold of 90% for the represented A_c, 15 targets are identified, as shown in Figure 4. These targets are derived from the data from DISCOS considering only spacecraft (no rocket bodies) in orbit between 700 and 1000 km, and launched in the last ten years. A reference breakup mass equal to $10\,000\,\mathrm{kg}$ was used. A propagation time of 25 years was considered.

As already presented in Figure 1, the cross-sectional area is not uniformly distributed across the whole LEO region: active satellites are mostly concentrated in polar orbits and

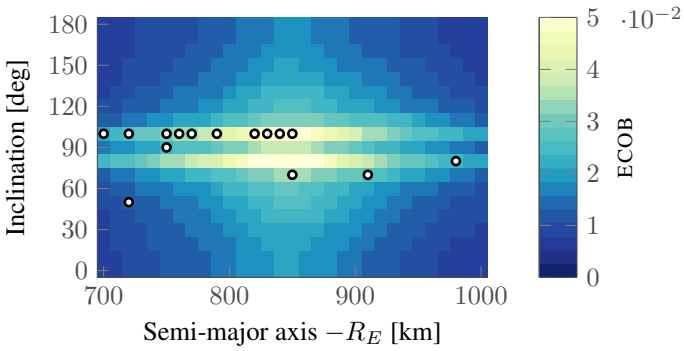

Fig. 4: Resulting index for catastrophic collisions with breakup mass equal to 10 000 kg. Collision probability measured on the 15 targets indicated by a marker. Propagation time equal to 25 years.

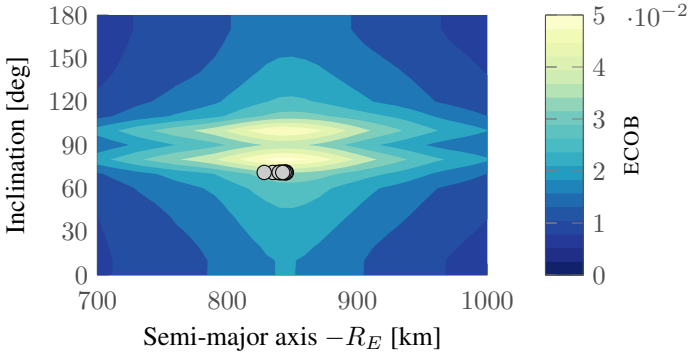

Fig. 5: Contour plot of the environmental index. The markers indicate the ten objects with the highest environmental index.

this explains the distribution of the targets in Figure 4. The concentration of targets at latitudes around 80 degrees results in a much higher index in these regions. For fragmentations at these latitude, the targets can spend a large part of their orbits in the area where the spatial density is maximum. For what concerns the semi-major axis, a high density of targets around 800-850 km makes this region the one with the highest environmental index.

The map in Figure 4 was combined with a database generated from DISCOS, which contains all objects in orbits between 700 and 1000 km, to evaluate the environmental index of objects already in orbit. Note that in this case, differently from the list used to define the target set, there is no filter on the launch date, and both rocket bodies (RB) and payloads (PL) are present.

As in Figure 4, Figure 5 represents the value of ECOB computed for a reference mass equal to 10 000 kg and propagation time equal to 25 years, but in this case a contour plot is used to represent the surface obtained with the interpolation. The markers indicate the ten objects with the highest environmental index among the ones in the database. In particular,

Table 1: Top ten objects with the largest environmental index ECOB among DISCOS data considering all objects in orbits between 700 and 1000 km. $\bar{h} = a - R_E$.

ID	COSPAR	Name	$\bar{h}$ [km]	i [deg]	Mass [kg]	ECOB
2	2004-021B	SL-16 R/B	845	71.0	9000	0.0329
3	2007-029B	SL-16 R/B	845	71.0	9000	0.0328
1	2000-006B	SL-16 R/B	841	71.0	9000	0.0327
7	1990-046B	SL-16 R/B	844	71.0	8226	0.0307
5	1992-093B	SL-16 R/B	842	71.0	8226	0.0307
10	1993-016B	SL-16 R/B	843	71.0	8226	0.0307
9	1988-102B	SL-16 R/B	840	71.0	8226	0.0305
4	1985-097B	SL-16 R/B	838	71.0	8226	0.0304
6	1987-041B	SL-16 R/B	835	71.0	8226	0.0302
8	1988-039B	SL-16 R/B	828	71.0	8226	0.0294

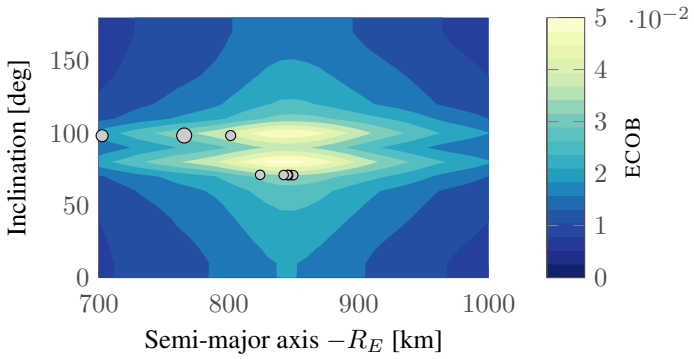

Fig. 6: Contour plot of the environmental index. The markers indicate the ten objects with the highest environmental index, considering only spacecraft launched more than ten years ago.

the location of the marker indicates the object orbital parameters and the size of the markers is proportional to the object mass. In this case, the markers have all similar size because all objects belong to the same family as shown in Table 1. The objects in Table 1 are sorted by the value of the environmental index ECOB, whereas the ID in the first column is related to the object mass, with ID $= 1$ for the most massive object in the database. All objects in Table 1 belong to the same family, SL-16 R/B: they combine high mass and orbits within the most critical regions.

The same analysis was performed also considering only spacecraft launched at least ten years ago. The results are shown in Table 2 and Figure 6. Also in this case, most objects belong to the same family (Cosmos satellites) with the exception of Envisat. It presents a much larger environmental index due to its large mass.

These two examples shows how the proposed environmental index gives an insight into the effect of different breakups on active satellites, highlighting the different contribution of mass, altitude, and inclination. However, it is also important to remind the limitations of the proposed index. The propagation method used for the fragment clouds considers only the effect of atmospheric drag, whereas at altitudes above 800 km solar radiation pressure is relevant

Table 2: Top ten objects with the largest environmental index ECOB among DISCOS data considering only spacecraft launched more than ten years ago and in orbits between 700 and 1000 km. $\bar{h} = a - R_E$.

ID	COSPAR	Name	$\bar{h}$ [km]	i [deg]	Mass [kg]	ECOB
20	2002-009A	Envisat	766	98.3	8111	0.0282
32	2002-056A	Cosmos 1656	801	98.3	3680	0.0189
39	1990-046A	Cosmos 2082	845	71.0	3221	0.0153
36	1984-106A	Cosmos 1603	846	71.0	3221	0.0152
34	1985-097A	Cosmos 1697	848	71.0	3221	0.0152
40	1988-039A	Cosmos 1833	842	71.0	3221	0.0152
38	1987-041A	Cosmos 1844	846	71.0	3221	0.0151
37	1987-027A	Cosmos 1943	850	71.0	3221	0.0151
35	1985-042A	Terra	824	71.1	3221	0.0143
25	1999-068A	Adeos 2	703	98.21	5190	0.0135

too. In addition, the propagation method limits the extent of the analysis both in altitudes (700-1000 km) and in time (maximum 25 years). Finally, no feedback effect can be considered with the current formulation. Some of these aspects are considered in alternative environmental indices, to which ECOB is compared in Section 6.

6. COMPARISON WITH OTHER FORMULATIONS

The proposed index ECOB was compared with some other environmental index formulations developed in the framework of the ESA study *Fragmentation Consequence Analysis for LEO and GEO Orbits*.

6.1. Comparison with FOM

FOM (Figure Of Merit) is an environmental index, developed by AIRBUS [2], with the following expression:

$$\text{FOM} = \Phi A_c M^{0.75} \Delta t_{\text{orb}} \tag{4}$$

where Φ is the debris flux in the object's orbit with units $[\text{m}^{-2}\,\text{yr}^{-1}]$, A_c and M are respectively the cross-sectional area and the mass of the object, Δt_{orb} [yr] is the remaining orbital lifetime.

The two indices were computed for the objects in Table 3. Note that it is more interesting to study the ranking obtained with the different approaches more than the numerical value of the indices. For this reason, the results were analysed studying the correlation between the methods, as shown in Figure 7. The results show a good coherence between the two methods except for the case of Envisat and MetOp-A. For Envisat, the large difference may be explained by the fact that FOM considers the *exposure* of the object to the background population (ΦA_c). This term is particularly relevant for Envisat as its orbit is within the most affected region by the Iridium-Cosmos fragmentation. On the other hand, the value for MetOp-A may be explained by how its orbital lifetime is computed in FOM. In fact, it is an operational spacecraft, so $\Delta t_{\text{orb}} = \Delta t_{\text{act}} + 25$, where Δt_{act} is the remaining mission duration. In this way, its orbital lifetime results much shorter than Envisat, even if MetOp-A is on a orbit with higher altitude. The distinction between active and not-active satellites is not trivial; moreover, one can be interested in evaluating the environmental impact of a spacecraft without considering post-disposal manoeuvres to assess how necessary those manoeuvres are. For this reason, active and inactive objects are treated in the same way in ECOB.

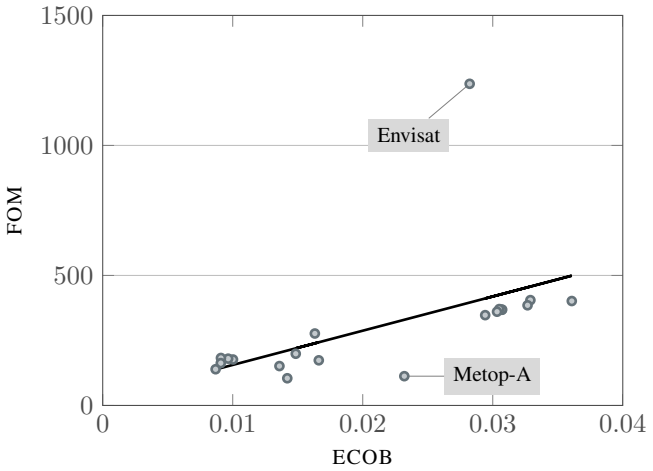

Fig. 7: Correlation between the proposed index ECOB and FOM.

6.2. Comparison with CSI

Rossi et al. [1] define a criticality index that takes into account four key-elements: environmental dependence, lifetime dependence, mass, and inclination. All these factors are combined in one index, Ξ, that is called the *Criticality of Spacecraft Index*. The expression of Ξ is

$$\Xi = \frac{M}{M_0} \frac{D(h)}{D_0} \frac{\text{life}(h)}{\text{life}(h_{1000})} \frac{1 + k\Gamma(i)}{1 + k},$$

where

- $\frac{M}{M_0}$ factors in the mass of the analysed spacecraft M, divided by a reference mass $M_0 = 10\,000\,\text{kg}$
- $\frac{D(h)}{D_0}$ considers the effect of the environment through $D(h)$, which is the spatial density of objects at the orbital altitude h, normalised by D_0, the spatial density of objects at 770 km
- $\frac{\text{life}(h)}{\text{life}(h_{1000})}$ compares the expected orbital lifetime of the object given its orbital altitude h to the orbital lifetime of an object with $h_{1000} = 1000\,\text{km}$
- $\frac{1+k\Gamma(i)}{1+k}$, with $k = 0.6$ and $\Gamma(i) = (1 - \cos i)/2$, considers the effect of inclination.

Table 3: 20 objects used for the comparison with FOM. Data from [17]. $\bar{h} = a - R_E$.

ID	COSPAR	Name	Type	$\bar{h}$ [km]	i [deg]	Mass [kg]	ECOB	FOM	Rank ECOB	Rank FOM
1	1998-043G	SL-16	RB	807.5	98.39	8226	0.0361	401.6	1	3
17	2004-021B	SL-16	RB	845	71	9000	0.0329	405.1	2	2
18	2000-006B	SL-16	RB	841	71	9000	0.0327	385.2	3	4
19	1990-046B	SL-16	RB	844	71	8226	0.0307	368.5	4	6
20	1992-093B	SL-16	RB	842.5	71.02	8226	0.0307	367.9	5	7
2	1998-045B	SL-16	RB	840	71.01	8226	0.0305	370.7	6	5
3	1987-027B	SL-16	RB	836.5	71	8226	0.0303	360.5	7	8
4	1988-039B	SL-16	RB	828.5	71.02	8226	0.0294	347.3	8	9
5	2002-009A	ENVISAT	PL	765.5	98.33	8111	0.0282	1236.9	9	1
6	2006-044A	METOP-A	PL	820.5	98.67	4086	0.0232	112.6	10	19
10	1999-008A	ARGOS	PL	828	98.71	2490	0.0166	173.6	11	15
9	1998-043A	RESURS O1-N4	PL	810.5	98.47	2775	0.0163	276.7	12	10
7	1998-045A	COSMOS 2360	PL	850.5	70.85	3171	0.0148	198.9	13	11
8	1989-089A	COBE	PL	877	98.98	2245	0.0142	104.6	14	20
11	1993-061A	SPOT 3	PL	828.5	98.85	1891	0.0136	151.5	15	17
15	1993-061H	ARIANE 40	RB	787	98.86	1764	0.0100	176.7	16	14
13	1998-017B	ARIANE 40	RB	780.5	98.46	1764	0.0096	180	17	13
12	1995-021B	ARIANE 40+	RB	766.5	98.73	1764	0.0091	182.6	18	12
16	1990-005H	ARIANE 40	RB	766	98.79	1764	0.0091	162.8	19	16
14	1991-050F	ARIANE 40	RB	756.5	98.7	1764	0.0087	139.3	20	18

Table 4: Comparison with the Criticality of Spacecraft Index as defined by Rossi et al. [1]. $\bar{h} = a - R_E$.

ID	Type	h [km]	i [deg]	Mass [kg]	Ξ	ECOB	Rank Ξ	Rank ECOB
10	RB	843.84	71	9000	0.139	0.032861	10	1
11	RB	843.44	70.98	9000	0.139	0.032803	11	2
13	RB	849.14	70.88	8226	0.135	0.030435	13	3
1	RB	994.04	99.25	9000	0.313	0.019288	1	4
9	PL	953.94	64.98	4955	0.143	0.010199	9	5
4	PL	963.94	65.04	4955	0.16	0.009499	4	6
15	PL	955.14	65.08	4500	0.131	0.009426	15	7
3	PL	964.94	64.99	4955	0.161	0.009424	3	8
14	PL	957.34	64.86	4500	0.134	0.009223	14	9
12	PL	958.44	64.7	4500	0.135	0.009114	12	10
7	PL	964.74	64.95	4500	0.146	0.008771	7	11
6	PL	968.34	65.28	4500	0.151	0.008637	6	12
8	PL	971.14	64.81	4500	0.145	0.008399	8	13
5	PL	977.04	64.49	4500	0.154	0.008065	5	14
2	PL	987.54	64.98	4500	0.163	0.007637	2	15

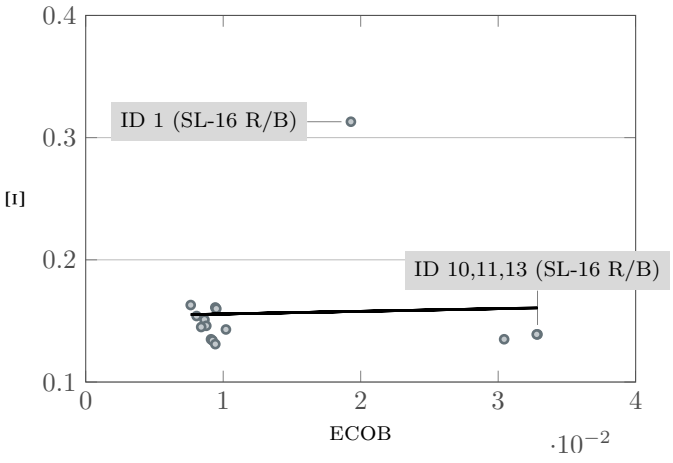

Fig. 8: Correlation between the proposed index ECOB and Ξ as defined by Rossi et al. [1].

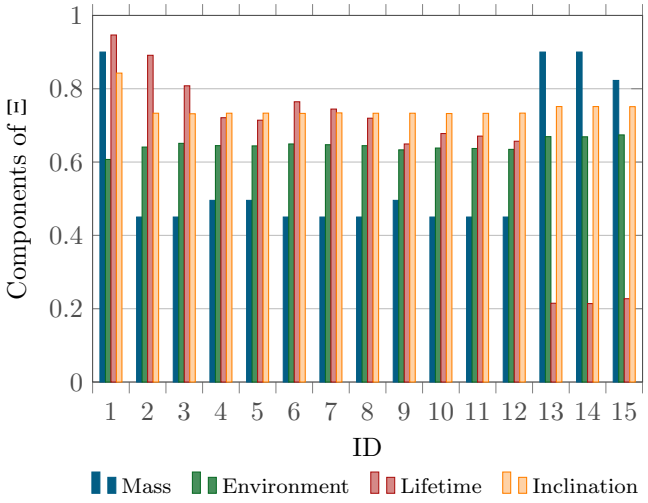

Fig. 9: Components of Ξ for the objects in Table 4.

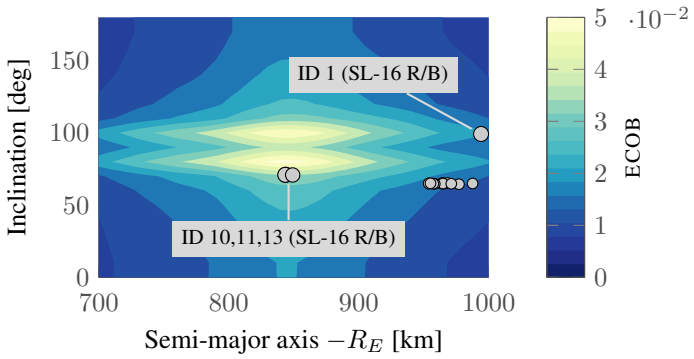

Fig. 10: Contour plot of the environmental index ECOB and objects from Table 4.

The objects evaluated by Rossi et al. [1] and their value of Ξ are listed in Table 4, where also the value of ECOB is reported. Figure 8 clearly shows that the two indices predict very different criticality for the objects in Table 4. In particular, a SL-16 R/B at high altitude presents a much higher criticality index than the others. The simple expression of Ξ allows to analyse in detail the reason of this result. Figure 9 compares the four components of Ξ for all the tested objects. The spacecraft with ID1 presents the largest mass, the longest lifetime, and the most critical inclination among all 15 objects. When ECOB is computed the mass and the inclination contribute to a large value of the criticality index, but the altitude actually reduces the criticality of the object. In fact, its orbit appears to be *far* from the ones with the largest effect on the selected targets (Figure 10). The opposite happens for the objects with ID 10, 11, 13, which have a large ECOB because they are in an orbital region with a large influence on the reference targets, but a small Ξ because of their orbital lifetime. The same observation explains the negative correlation in the cluster of objects in the bottom left of Figure 8: for these objects, ECOB increases when their altitude decreases because their distance from the targets' orbits decreases, whereas Ξ increases if the altitude increases. This observation reflects the fact that two indices are measuring the environmental impact on two distinct set of objects: ECOB only active satellites in a *medium* term timespan, whereas Ξ on the whole LEO region with an indefinite timespan. Both descriptions are possible, but it should be clarified which is more relevant to rank the criticality of space objects.

7. APPLICATION

As introduced at the beginning of the paper, environmental indices for spacecraft are often proposed to identify potential candidates for active debris removal mission. In addition, an environmental index could also be used, prior to launch, to support the licensing phase in the evaluation of the planned post-mission disposal strategies. For example, a licence system connected to an environmental index can distinguish between a CubeSat in orbit at 700 km at low inclination and a 4000 kg satellite in a polar orbit at 800 km. As the environmental impact of a potential breakup involving the two spacecraft is different, a higher level of reliability of the post-mission disposal may be requested in the latter case.

To apply the index for this purpose, it may be useful to translate the numerical value of the index into a *scale* that can communicate immediately the level of risk associated with an object. This has already been done in the case of asteroids, with the Torino [18] and the Palermo [19] scale. In the case of asteroids, the scales take into consideration both the effects of an impact and its likelihood to happen. The index proposed in this work looks only at the effects of the fragmentations, so the derived scale will be similar to the ones

Table 5: Definition of severity categories [20] and possible meaning for the description of the consequences of a breakup.

Severity	Dependability effects	Safety effects	Breakup consequences	Symbol
Catastrophic	Failure propagation	Severe detrimental environmental effects	Subsequent collisions	
Critical	Loss of mission	Major detrimental environmental effects	Major increase in collision risk	
Major	Major mission degradation		Increase in coll. avoidance manoeuvres	
Minor	Minor mission degradation		Negligible	

used for earthquakes, where only the severity of the events is evaluated. Following the analogy with earthquakes, levels of expected effects of the breakups can be defined. A possible definition can be derived from the severity levels used in the FMECA (Failure Modes, Effects, and Criticality Analysis) applied during the quality assessment of space missions [20]. Four levels of severity are defined, as summarised in Table 5. An example of the translation of these levels to the case of fragmentations is provided in the same table.

As the value of ECOB depends on the population of active satellites used to build the set of target objects, the connection between the environmental index and the severity levels cannot be done by setting a simple numerical threshold for the index. A reference fragmentation may be identified as a threshold for each level, as in the example shown in Table 6. Note that the fragmentations in Table 6 are only an example to explain how the relationship between the index and the severity levels can be built; further analysis is required to evaluate the most appropriate reference fragmentations. The analysis of fragmentations with similar orbital parameters would also enable to study how the produced number of fragments is related to the increase in collision warnings and collision avoidance manoeuvres. This analysis is left for future work.

Once the thresholds are defined, the value of the index can be associated to a severity level. Figure 11 shows the resulting severity level associated with some representative space objects: the colour indicates the different severity levels as defined in Table 5 and the vertical lines refers to the threshold vlaues defined in Table 6. Out of the ten cases represented,

Table 6: Definition of representative fragmentations as thresholds for the severity categories.

Threshold	Object	m [kg]	h [km]	i [deg]	ECOB
Minor/Major	Iridium	560	780	86.39	0.0035
Major/Critical	Fengyun 1C	1350[1]	865	98.65	0.0103
Critical/Catastrophic	Envisat	8111	766	98.3	0.0282

[1] The value includes the mass of the satellite and the one of the projectile.

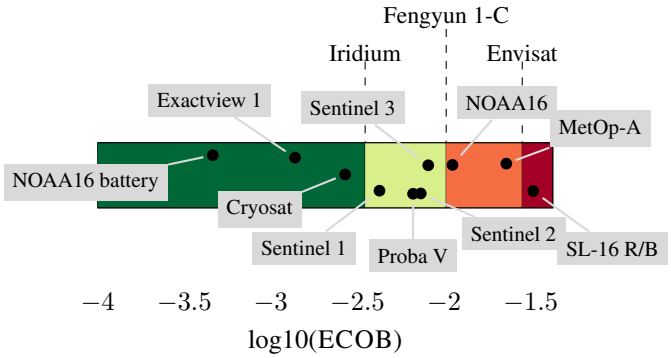

Fig. 11: Example of severity classification for several representative missions. The colours refer to the levels defined in Table 5.

Severity category	SNs	Probability level			
		10^{-5}	10^{-3}	10^{-1}	1
		PNs			
		1	2	3	4
catastrophic	4	4	8	12	16
critical	3	3	6	9	12
major	2	2	4	6	8
negligible	1	1	2	3	4

Fig. 12: Criticality matrix as defined in [20].

eight refer to spacecraft, one to a SL-16 rocket body with parameters as in Table 1, and one case (*NOAA16 battery*) where only the fragmentation of a component of small mass (20 kg in this example) is considered.

The purpose of this classification is then to estimate if the potential breakup of a spacecraft should be consider *critical*. Referring again to [20], the estimation of the criticality is done as shown in Figure 12 by combining the description of the effects with the severity categories and the probability level of the event. For the case of fragmentations, the probability level may be estimated considering the flux of debris objects on the spacecraft, within an appropriate time scale (e.g. 100 years), after the end of the mission and according to the proposed mitigation measure. If an object belongs to one the orange cells, the proposal of a different mitigation strategy may be suggested. Additional analysis may be performed in the scenario with no mitigation strategy to assess the requested reliability level on the disposal.

8. CONCLUSIONS

This paper proposed an environmental index based on the assessment of the effect of breakups on operational satellites. The population of operational satellites is analysed by considering the distribution of the spacecraft cross-sectional area in semi-major axis and inclination, for satellites in orbit between 700 and 1000 km. The distribution was sampled in a

such a way to obtain a set of representative targets, whose trajectories are propagated and which are used to compute the collision probability due to the simulated fragmentation.

For the fragmentation initial conditions, a variation in semi-major axis, inclination, and mass is considered. The simulated breakup is a catastrophic collision so that, applying the NASA breakup model, a direct dependence of the number of produced fragments on the fragmenting mass can be included. Once the debris cloud is generated, its density is propagated by applying the analytical method CiELO to describe the effect of atmospheric drag. Given the spatial density of the cloud, the collision probability of the targets is obtained by applying the kinetic theory of gases. The sum of the cumulative collision probability over 25 years for all the representative targets gives the value of the environmental index. The index is computed for some defined grid points in semi-major axis and inclination, whereas the values for different masses can be derived by simply rescaling the results corresponding to a reference mass value. The environmental index for a generic space object is obtained by interpolation of the values on the grid points.

The environmental index was assessed for all the objects present in the DISCOS database and in orbit between 700 and 1000 km. The results appear consistent and highlight the contribution of the inclination, with maximum values of the environmental index for the fragmentations occurring at orbital inclinations close to the targets' one. Also the fragmentation altitudes affects the environmental index, which is higher for altitudes close to the ones populated by operational spacecraft.

The proposed environmental index was compared to other formulations proposed in the literature, which consider different aspects of the problem. An explanation of the differences in the results was proposed. The comparison also suggests the importance of a clear definition of the scope and purpose of environmental indices to identify which aspects are essential to their definition.

Finally, it was shown how an environmental index may be included in the licensing phase of a spacecraft, assessing the criticality of its breakup.

References

[1] A. Rossi, G. B. Valsecchi, and E. M. Alessi, "The Criticality of Spacecraft Index," *Advances in Space Research*, vol. 56, no. 3, 2015, special Issue: Advances in Asteroid and Space Debris Science and Technology - Part 1. [Online]. Available: http://dx.doi.org/10.1016/j.asr.2015.02.027

[2] J. Utzmann, M. Oswald, S. Stabroth, P. Voigt, and I. Retat, "Ranking and characterization of heavy debris for active removal," in *63rd International Astronautical Congress*. International Astronautical Federation, Sep. 2012, iAC-12-A6.2.8.

[3] B. Bastida Virgili and H. Krag, "Active Debris Removal for Leo Missions," in *Sixth European Conference on Space Debris*, L. Ouwehand, Ed. ESA Communications, Aug. 2013, pp. 22–25.

[4] T. Lang, R. Destefanis, L. Evans, L. Grassi, S. Kempf, F. Schaefer, and T. Donath, "Assessing Debris Mitigation Efficiency Using Risk- Oriented Criteria : Application To Leo European Mission," in *Sixth European Conference on Space Debris*, L. Ouwehand, Ed. ESA Communications, Aug. 2013, pp. 22–25.

[5] A. Rossi, H. G. Lewis, A. E. White, L. Anselmo, C. Pardini, H. Krag, and B. Bastida Virigili, "Analysis of the consequences of fragmentations in Low and Geostationary orbits," *Advances in Space Research*, 2015. [Online]. Available: http://dx.doi.org/10.1016/j.asr.2015.05.035

[6] H. G. Lewis, "ACCORD: Alignment of Capability and Capacity for the Objective of Reducing Debris," University of Southampton, FP7 Final Report, 2014. [Online]. Available: http://cordis.europa.eu/docs/results/262/262824/final1-accordfinalreportsection4-1.pdf

[7] P. H. Krisko, "Proper Implementation of the 1998 NASA Breakup Model," *Orbital Debris Quarterly News*, vol. 15, no. 4, pp. 1–10, 2011. [Online]. Available: http://orbitaldebris.jsc.nasa.gov/newsletter/pdfs/ODQNv15i4.pdf

[8] F. Letizia, C. Colombo, and H. G. Lewis, "Analytical model for the propagation of small debris objects clouds after fragmentations," *Journal of Guidance, Control, and Dynamics*, vol. 38, no. 8, pp. 1478–1491, 2015. [Online]. Available: http://arc.aiaa.org/doi/abs/10.2514/1.G000695

[9] N. L. Johnson and P. H. Krisko, "NASA's new breakup model of EVOLVE 4.0," *Advances in Space Research*, vol. 28, no. 9, pp. 1377–1384, 2001. [Online]. Available: http://www.sciencedirect.com/science/article/pii/S0273117701004239

[10] C. R. McInnes, "An analytical model for the catastrophic production of orbital debris," *ESA Journal*, vol. 17, no. 4, pp. 293–305, 1993.

[11] F. Letizia, C. Colombo, and H. G. Lewis, "Multidimensional extension of the continuity equation method for debris clouds evolution," *Advances in Space Research*, 2015. [Online]. Available: http://www.sciencedirect.com/science/article/pii/S0273117715008327

[12] Orbital Debris Program Office, "History of on-orbits satellite fragmentations," May 2014, [Online] Retrieved on 26/08/2015. [Online]. Available: http://orbitaldebris.jsc.nasa.gov/library/satellitefraghistory/13theditionofbreakupbook.pdf

[13] D. J. Kessler, "Derivation of the collision probability between orbiting objects: the lifetimes of Jupiter's outer moons," *Icarus*, vol. 48, no. 1, pp. 39–48, Oct. 1981. [Online]. Available: http://linkinghub.elsevier.com/retrieve/pii/0019103581901512

[14] F. Letizia, C. Colombo, and H. G. Lewis, "Collision probability due to space debris clouds through a continuum approach," *Journal of Guidance, Control, and Dynamics*, 2015, accessed 10 September 2015. [Online]. Available: http://arc.aiaa.org/doi/abs/10.2514/1.G001382

[15] S. Valk, A. Lemaître, and F. Deleflie, "Semi-analytical theory of mean orbital motion for geosynchronous space debris under gravitational influence," *Advances in Space Research*, vol. 43, no. 7, pp. 1070–1082, Apr. 2009. [Online]. Available: http://www.sciencedirect.com/science/article/pii/S0273117708006807

[16] T. Flohrer, S. Lemmens, B. Bastida Virgili, H. Krag, H. Klinkrad, E. Parrilla, N. Sanchez, J. Oliveira, and F. Pina, "DISCOS - Current status and future developments," in *Sixth European Conference on Space Debris*, L. Ouwehand, Ed. ESA Communications, Aug. 2013.

[17] J. Radtke, C. Kebschull, S. Flegel, V. Braun, F. Schäfer, M. Rudolph, and J. Utzmann, "Fragmentation consequence analysis for leo and geo orbits," Technische Universität Braunschweig, Tech. Rep. ESA Contract No. 4000106517/12/F/MOS, Sep. 2014.

[18] D. Morrison, C. R. Chapman, D. Steel, and B. R. P, "Impacts and the public: Communicating the nature of the impact hazard," in *Mitigation of Hazardous Comets and Asteroids*. Cambridge University Press, 2004.

[19] S. R. Chesley, P. W. Chodas, A. Milani, G. B. Valsecchi, and D. K. Yeomans, "Quantifying the risk posed by potential earth impacts," *Icarus*, vol. 159, no. 2, pp. 423–432, 2002.

[20] European Cooperation for Space Standardisation, "Space product assurance: Failure modes, effects (and criticality) analysis (FMEA/FMECA)," ESA Requirements and Standards Division, Tech. Rep. ECSS-Q-ST-30-02C, Mar. 2009.